Improving EEG Muscle Artifact Removal With an EMG Array

Juan Andrés Mucarquer, Pavel Prado, María-José Escobar, Wael El-Deredy, and Matías Zañartu, *Senior Member, IEEE*

***Abstract*— Removal of artifacts induced by muscle activity is crucial for analysis of the electroencephalogram (EEG), and continues to be a challenge in experiments where the subject may speak, change facial expressions, or move. Ensemble empirical mode decomposition with canonical correlation analysis (EEMD-CCA) has been proven to be an efficient method for denoising of EEG contaminated with muscle artifacts. EEMD-CCA, likewise the majority of algorithms, does not incorporate any statistical information of the artifact, namely, electromyogram (EMG) recorded over the muscles actively contaminating the EEG. In this paper, we propose to extend EEMD-CCA in order to include an EMG array as information to aid the removal of artifacts, assessing the performance gain achieved when the number of EMG channels grow. By filtering adaptively (recursive least squares, EMG array as reference) each component resulting from CCA, we aim to ameliorate the distortion of brain signals induced by artifacts and denoising methods. We simulated several noise scenarios based on a linear contamination model, between real and synthetic EEG and EMG signals, and varied the number of EMG channels available to the filter. Our results exhibit a substantial improvement in the performance as the number of EMG electrodes increase from 2 to 16. Further increasing the number of EMG channels up to 128 did not have a significant impact on the performance. We conclude by recommending the use of EMG electrodes to filter components, as it is a computationally inexpensive enhancement that impacts significantly on performance using only a few electrodes.**

***Index Terms*— Adaptive filtering, artifact removal, blind-source-separation, electroencephalogram (EEG), electromyogram (EMG), muscle artifacts.**

I. Introduction

THE electroencephalogram (EEG) is an electrophysiological technique for recording the electrical activity of the brain by placing electrodes on the scalp. EEG signals consist of differences in electrical potentials between a reference electrode and the electrode array. Among the various brain imaging techniques, EEG has a very high time resolution, enabling the study of sensory and cognitive processes in the time scale in which they occur. The broad adoption of the EEG in the biomedical and scientific domains includes its use for diagnosis, analysis, and brain–computer interfaces (BCIs) [1]. The electrical field emanated by the brain activity passes through the skull and reaches the electrodes (by physical volume conduction), rendering a low signal-to-noise ratio (SNR) for brain signals, with a spectrum in the range of 0.01–100 Hz [1]. Muscle activity is considered the primary physiological artifact source in the EEG, as they also emanate electrical activity that reaches the electrodes. In most cases, muscular sources are closer to scalp electrodes than the brain, contributing significant energy with broad spectral noise source. Proper removal of muscle artifacts is crucial for achieving real neurofeedback training, constructing efficient BCI, and making reliable analyses of brain potentials. Muscle contamination is a serious concern in the EEG, especially since it has been recently shown that these undesired signals could perfectly mimic brain activity in neurofeedback training [2], becoming especially critical when estimating EEG sources under conditions that involve intense muscle activity, such as changing facial expressions, walking, exercising, and speaking.

We summarize the hallmarks of muscle interference in two main situations. First, single motor units (SMUs) activations are found in all EEG electrodes without time delay [3] (at least when sampling the EEG below 1 kHz), due to volume conduction, and where the SMUs' activation is present even in resting state conditions [3]. In addition, studies involving partial induced or total paralysis are supporting reasons for considering the background myogenic activity as noise [4], [5]. The second situation is the spectral overlap between muscle and brain signals. Muscles' activation appears in a burst, present tonic, and spontaneous components and has different spectral signatures across individual and group muscles [6]. Nevertheless, brain signals are known to be much more autocorrelated (at lag 1) than muscle signals. For instance, the activity of temporal and frontalis muscles can be modeled as a white noise process, due to the presence of power in all EEG frequencies [as the electromyogram (EMG) spectrum is in the range of 0.01–200 Hz] [7].

In addition to these two characteristics of signal interferences, the absence of ground truth for brain and muscle signals makes the quantification of the distortions (induced by muscles and artifact removal algorithms) a difficult problem [4], [8]–[12]. To validate and compare different

Manuscript received October 19, 2018; revised January 24, 2019; accepted March 4, 2019. Date of publication May 1, 2019; date of current version February 10, 2020. This work was supported in part by the Comisión Nacional de Investigación Científica y Tecnológica (CONICYT) under Grant FONDECYT 1151077, Grant BASAL FB0008, and Grant ANILLO ACT172121, and in part by the National Institute on Deafness and Other Communication Disorders, National Institutes of Health under Award P50DC015446. The Associate Editor coordinating the review process was Sabrina Grassini. *(Corresponding author: Juan Andrés Mucarquer.)*

J. A. Mucarquer, M.-J. Escobar, and M. Zañartu are with the Department of Electronic Engineering, Universidad Técnica Federico Santa María, Valparaíso 2390123, Chile (e-mail: juan.mucarquer@usm.cl; mariajose.escobar@usm.cl; matias.zanartu@usm.cl).

P. Prado is with the Advanced Center for Electrical and Electronic Engineering, Universidad Técnica Federico Santa María, Valparaíso 2390123, Chile (e-mail: pavel.prado@usm.cl).

W. El-Deredy is with the Department of Biomedical Engineering, Universidad de Valparaíso, Valparaíso 2360102, Chile (e-mail: wael.el-deredy@uv.cl).

Digital Object Identifier 10.1109/TIM.2019.2906967

method to remove EMG artifacts, simulations assuming a contamination model are performed, using real and synthetic signals. Although validation procedures on experimental recordings have been proposed [13], they rely on using two or more instruments (EEG + functional near-infrared spectroscopy or magnetoencephalogram), to obtain a highly correlated signal for estimating an EEG ground truth.

A. Current Muscle Artifact Removal Methods

Most of the relevant techniques for muscular artifact removal relies on solving a linear blind source separation (BSS) problem, using algorithms such as independent component analysis (ICA) [14] and canonical correlation analysis (CCA) [7], [15]. Typically, the procedure consists of decomposing the EEG array into N sources, where the artefactual sources are identified and removed, and the remaining sources (artifact-free) are projected back onto the EEG array. This procedure is often made by manual inspection of artefactual sources, and although automatization methods have been proposed, it is impossible to assure that found sources are either pure artifacts or brain components, leading to potential information loss and brain signal attenuation.

More specifically, the technique used to solve the BSS problem depends on artifact characteristics. In the domain of ocular artifact removal, ICA has shown better performance [16] (less error in reconstructing simulated signals with realistic ocular noise), because the ocular movement artifact is stereotyped and does not resemble a Gaussian noise. Note that solving BSS through ICA is, in essence, to maximize the non-Gaussianity of the sources [17]. For removal of temporal and frontalis muscle activity, CCA has shown better performance [7], [15], since the activity of those muscles is fast, appears in bursts, and is much less autocorrelated than brain signals (CCA aims to find sources that are maximally autocorrelated). Chen *et al.* [18] proposed the use of independent vector analysis (IVA) for the removal of muscle artifacts. IVA is a technique that aims to take advantage of both ICA and CCA, outputting sources that are consistently dependent among several data sets and, at the same time, independent of each other within a data set. Although it is reported to outperform ICA and CCA for mild to good SNRs (>0 dB), it requires multiple data sets and the computation time is at least 50 times larger than ICA.

In addition, BSS requires a multichannel array, and it generally assumes that the number of sources is less or equal than the number of electrodes. Moreover, this estimation problem could be considered underdetermined when, e.g., the number of sources exceeds the number of EEG electrodes; and by the same reason, it is generally accepted that a higher number of channels would lead to better performance [19]. The hybrid single-channel variation of BSS-CCA proposed in [15] is composed of two main steps. First, using ensemble empirical mode decomposition (EEMD), the EEG channel is decomposed into multiple components. Second, BSS is applied to the resulting matrix (CCA), canceling the sources that are assumed to be mostly artifacts, for finally backproject the artifact-free components and apply inverse EEMD on those.

The discussion on whether a single-channel or multichannel technique is more suitable for the artifact removal problem was recently investigated for facial muscle artifacts [19]. In this paper, multichannel BSS-CCA and single-channel EEMD-CCA are compared, and the single-channel technique achieved better results when reconstructing signals. The authors suggested that a possible reason behind this finding could be the high variability in the number of sources. Thus, using more channels and assuming a square mixing matrix B can lead to mixing up more myogenic and brain sources than separating them. Following this idea, two hybrid algorithms were proposed, based on the same decomposition steps of a single electrode and then BSS was applied. Maddirala and Shaik [20] decomposed a single electrode using singular spectrum analysis (SSA) and then applied ICA (SSA-ICA). The authors reported that decomposing the signal using SSA performed better than Wavelet-ICA [21], EEMD-ICA [14], and SSA-adaptive noise canceller [22]. In [23], a method to utilize the interdependency information on surrounding electrodes was proposed. This idea was performed by decomposing a reduced number of EEG channels (three to eight) by means of multivariate EMD (MEMD) and then applying CCA. Their results performed better than single-channel EEMD-CCA thus indicating that the multichannel approach can, in fact, introduce the expected performance enhancement if handled properly.

Summarizing, the majority of research addressing the muscle artifact removal problem focus on limited sensing capabilities, giving additional support to single-channel techniques due to their inherent instrumental simplicity and clinical applicability. In this paper, we explore if the best performance in the literature could be improved by adding statistical information of the artifact by using an EMG electrode array. For this end, we extended a well-established single-channel method (EEMD-CCA) to include the EMG array by making regression on the found sources adaptively. Our goal is to enable the user to make natural facial expressions and talk during the EEG experiment. It is worth remarking that the scope of the method we describe only takes into consideration EMG signals synchronously recorded with EEG, thus allowing zero-lag interference removal.

This paper is structured as follows. Section II introduces the methods and the proposed scheme in detail. Section III describes the data sets used as well the data generation, the contamination model and performance measures. Section IV presents and discusses the results for the various simulation conditions along the validity of the study. Section V concludes our study with recommendations regarding the use of EMG electrode-arrays on EEG experiments that involve subject movement.

II. Methods

A. EEMD Expansion

Empirical mode decomposition (EMD) decomposes a signal into a variable number of intrinsic mode functions (IMFs). Each IMF satisfies two conditions: 1) the difference between the number of zero crossings and extreme values must be less

than or equal to one and 2) for all time points, the average of the upper and lower envelopes is zero. The first IMF c_1 is obtained by subtracting the average between the upper and lower envelopes of the original signal y recursively, until the resulting signal satisfies the IMF conditions. When an IMF is found, it is subtracted from the original signal, obtaining a residual $r_1 = y - c_1$. The same procedure is then applied to the residual r_1, in order to obtain a second IMF c_2, and so on. The iteration stops when the residual signal r_P becomes a monotonic function, giving the number of resulting IMFs (P). The original signal can be reconstructed by summing all IMFs and the last residual c_P, i.e., $y = \sum_{i=1}^{P} c_i + r_P$.

EEMD [24] is a variation of the previous algorithm that is more robust against noise and outliers. A fixed number (I) of ensembles is chosen (ten or more according to [19]). Following, EMD is applied I times on the original signal with added independent identically distributed (i.i.d.) noise whose variance is equal to 0.2 times the original signal variance [24]. I ensembles of P IMFs are obtained, for then averaging all of them. The implementation of EEMD used is libeemd [25], which is freely available as open source software.

B. Multichannel BSS-CCA

The BSS problem assumes that $Y(k) = BS(k)$, where $B \in \mathbb{R}^{N\times N}$ is the mixing matrix, and, $Y(k), S(k) \in \mathbb{R}^{N\times T}$ are the EEG data matrix (in the EEMD-CCA algorithm, the multichannel output of EEMD over a single electrode) and the sources, respectively. The goal is to find $W \approx B^{-1}$ in order to obtain an approximation of the sources by $\tilde{S}(k) = WY(k)$. CCA is one way to solve the BSS problem, by constraining the sources to be maximally autocorrelated (at a specific lag) and mutually uncorrelated.

Define $Y_1(k)$ as a delayed version of the original data matrix, i.e., $Y_1(k) = Y(k-1)$. CCA aims to maximize the correlation between linear combinations of Y and Y_1

$$\max_{w_0,w_1} \rho(w_0^T Y, w_1^T Y_1) = \frac{w_0^T \Sigma_{01} w_1}{\sqrt{(w_0^T \Sigma_{00} w_0)(w_1^T \Sigma_{11} w_1)}} \quad (1)$$

where $w_0, w_1 \in \mathbb{R}^N$. Σ_{00}, Σ_{11} are the autocovariance matrices of Y and Y_1, respectively, and Σ_{01} is the covariance matrix between them.

It can be proven that the optimization problem mentioned earlier reduces to the following eigenproblem:

$$\begin{cases} \Sigma_{00}^{-1}\Sigma_{01}\Sigma_{11}^{-1}\Sigma_{10} w_0 = \rho^2\ w_0 \\ \Sigma_{11}^{-1}\Sigma_{10}\Sigma_{00}^{-1}\Sigma_{01} w_1 = \rho^2\ w_1 \end{cases} \quad (2)$$

giving the first pair of canonical variates $w_0^T Y$ and $w_1^T Y_1$. The next pairs of canonical variates (i.e., $\{w_2^T Y, w_3^T Y_1\}, \{w_4^T Y, w_5^T Y_1\}$, and so on) can be obtained solving the same eigenproblem, by adding the constraint of being orthogonal to the previous canonical variates.

The source matrix $\tilde{S}(k)$ is constructed by concatenating the first of each pair of canonical variates obtained by (2) as rows. The sources are sorted from high to low autocorrelation. With the assumption that the least autocorrelated sources are mostly of myogenic origin, a threshold on the autocorrelation of the sources is applied to separate myogenic and brain sources.

The implementation of CCA used in this study is included on the FieldTrip Toolbox for MATLAB [26].

C. Adaptive Filter Over BSS

CCA aims to find sources (linear combinations of the measurements) that are maximally autocorrelated and mutually uncorrelated, taking advantage of the knowledge that brain signals are highly autocorrelated. A threshold on the autocorrelation of resulting sources is applied, then the least autocorrelated sources are assumed to be pure artifacts and thus set to zero.

The proposed scheme filters the sources adaptively (using a recursive least-squares filter) instead of removing some of them, by subtracting the contribution of a reference signal (EMG electrodes), according to a linear model of interference. This is a more subtle way to process the artefactual sources than setting them to zero and thus, helping to mitigate the potential information loss issue in BSS.

Let N be the number of resulting artefactual sources, represented by $\tilde{s}_n(k) \in \mathbb{R}^T, n \in \{1, \ldots, N\}$.

Over the assumption that EMG signals are positioned sufficiently far for not capturing any brain signals and that activations of EMG signals are immediately visible on all EEG electrodes, a linear model of interference was proposed [27]

$$\tilde{s}_n(k) = s_n(k) + X^T(k)\Theta \quad (3)$$

where $s_n(k)$ is the true EEG source and $X(k) = [x_1(k), \ldots, x_{N_M}(k)]^T$ is the EMG data matrix. In addition, $\Theta \in \mathbb{R}^{N_M}$ are the coefficients in which every EMG electrode x_j influences (linearly) the EEG electrode y_i in question. These coefficients are expected to behave inversely proportional to the distance, by assuming that the interference of distant EMG electrodes has less reflection amplitude than the close ones to the EEG electrode.

The extended recursive least-squares (ERLS) algorithm [16], [28] is proposed to find the parameters Θ for each artefactual source $\tilde{s}_m(k)$ by

$$\epsilon(k) = \tilde{s}_m(k) - X^T(k)\hat{\Theta}(k-1) \quad (4)$$

$$r_\epsilon(k) = \beta^k + X^T(k)P(k-1)X(k) \quad (5)$$

$$\hat{\Theta}(k) = A\hat{\Theta}(k-1) + \kappa(k)\epsilon(k) \quad (6)$$

$$\kappa(k) = AP(k-1)X(k)/r_\epsilon(k) \quad (7)$$

$$P(k) = A[P(k-1) - P(k-1)X(k)X^T(k) P(k-1)/r_\epsilon(k)]A^T + \beta^k q I \quad (8)$$

where $\epsilon(k)$ is the error signal, $\kappa(k)$ is the weight for parameter updating, $\hat{\Theta}(k)$ is for the current estimation of Θ, and $P(k)$ is the EMG autocovariance matrix. In addition, the parameter β is the forgetting factor of the ERLS and q is a weight between model variation and measurement disturbances.

The filtered source $\hat{s}_n(k)$ can be thus obtained by

$$\hat{s}_n(k) = \tilde{s}_n(k) - X^T(k)\hat{\Theta}(k). \quad (9)$$

This filtering process is repeated for every artefactual source $n \in \{1, \ldots, N\}$, constructing a filtered BSS source

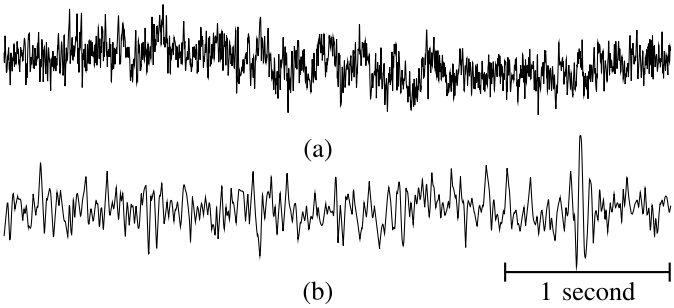

Fig. 1. (a) RealEEG channel Cz and (b) SimEEG 4-s window sample.

matrix $\hat{S}(k)$. Inverse BSS is applied by $\hat{Y}(k) = B\hat{S}(k)$, to finally, sum the rows of $\hat{Y}(k)$ (inverse EEMD) thus, yielding the filtered single EEG channel $\hat{y}_i(k)$.

The implementation of the ERLS filter is an in-house MATLAB R2018a script.

III. Data Set Description, Simulations, and Performance Comparison

Two EEG data sets were used to test the proposed method. The first data set consists of 32-channel of EEG recorded from two subjects involved in a passive listening task (auditory oddball paradigm during hypnosis), obtained from BNCI Horizon 2020 Project, freely available under Creative Commons license.[1] Eye-motion artifacts were removed using ICA and setting to zero the components by manual inspection. The resulting clean EEG is called RealEEG. In order to have an additional realization of a clean EEG signal, we simulated a second data set using SimEEG software [29], which implements a wavelet analysis approach on real EEG signals in order to generate EEG data with similar spectral composition (simulated EEG bands activity). This data set is labeled as SimEEG. Both data sets are considered to be clean of artifacts and were divided into 4-s windows ($T = 2048$ samples), for then normalizing each window, subtracting their mean and dividing by their standard deviation. The selection of the 4-s window length is based on the interest to compare our results with the literature, e.g., the original EEMD-CCA [15], [19], where the window length was always 4 s. Two sample windows for RealEEG and SimEEG are shown in Fig. 1.

EMG signals were recorded from a subject in resting state and in an exercise of vocalization, uttering a set of long syllables. The signals were acquired using eight EMG electrodes sampled at 8192 Hz, distributed uniformly around the cheeks and neck of the subject. Postprocessing of these signals included downsampling to 512 Hz, a bandpass filter between 0.1 and 256 Hz, and electrocardiogram removal is done manually using ICA. Signals were divided in 4-s windows that were Z-score normalized by removing their mean and dividing by their standard deviation. These signals were treated as muscular sources and called RealEMG. A second data set of EMG muscular sources was simulated to resemble typical EEG simulations [19], [30], i.e., spontaneous bursting behavior of Gaussian noise. Herein, every source is a train of impulses drawn from a Poisson process, with impulse amplitudes uniformly distributed between 0 and 1. The bursting behavior was obtained by passing a sliding window, setting the window to 0 (no activations) if there are 2 or less activation inside the window. Each train of impulses is then convolved by Gaussian noise, with variance equal to the amplitude of the impulse and random duration between 100 and 500 ms, uniformly chosen. Twenty-five windows of 4-s length were simulated and called SimEMG. To match the number of sources available by EMG measurements, $N_M = 8$ sources were generated. The number of sources will be discussed at the end of this paper. A sample window of these sources is shown in Fig. 2.

[1] http://bnci-horizon-2020.eu/database/data-sets

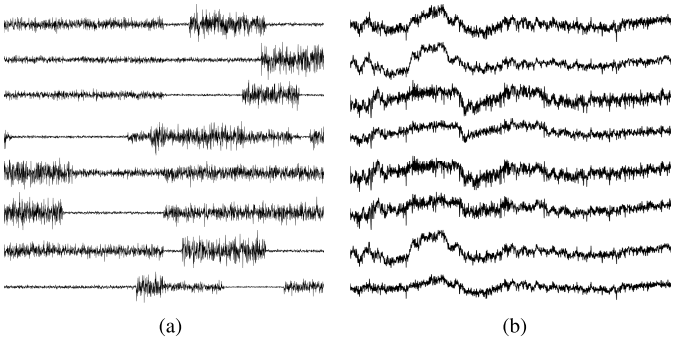

Fig. 2. Sample of 4 s of eight-channel. (a) SimEMG. (b) RealEMG.

A. Contamination Model

A linear model of contamination is proposed between clean EEG signals y_i (a 4-s window) and both RealEMG and SimEMG $X \in \mathbb{R}^{N_M \times T}$. First, we mixed the muscular sources multiplying them by a random matrix $C \in \mathbb{R}^{N_M \times N_M}$, for then sum every row $(CX)_j$ to obtain an artifact $a(k)$, which is added to the clean EEG window. The λ parameter is used to control the SNR between artifact and ground truth EEG. One clean EEG channel i, $y_i(k)$ was contaminated by the sum of all EMG channels $x_j(k)$, as shown in (11)

$$a(k) = \sum_{j=1}^{N_M} (CX)_j \tag{10}$$

$$\tilde{y}_i(k) = y_i(k) + \lambda a(k). \tag{11}$$

The SNR and the root mean squared (rms) value is defined as follows:

$$\text{SNR} = 10 \log \frac{\text{rms}(y_i)}{\text{rms}(\lambda a)} \tag{12}$$

$$\text{rms}(x) = \sqrt{\frac{1}{T} \sum_{k=1}^{T} x^2(k)}. \tag{13}$$

In order to test the algorithms in a high-noise environment, we set eight values of λ to obtain SNRs in the range of -10–1 dB. For the same reason, to increase nonstationarity, a new C matrix was drawn on every window. Table I summarizes the signals used in the simulation trials and Fig. 3 presents a window sample of each signal for the worst SNR (-10 dB).

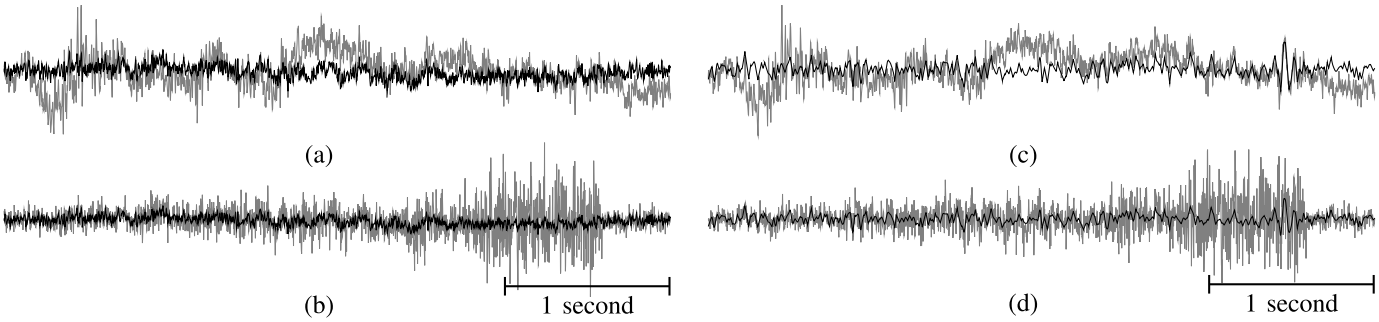

Fig. 3. Contaminated signal samples for all data sets used in simulations, for SNR = −10.5 dB. (a) S_1. (b) S_2. (c) S_3. (d) S_4. Black line: ground truth signal (artifact-free EEG). Superimposed gray: contaminated signal.

TABLE I
DESCRIPTION OF SIGNALS IN SIMULATIONS

Dataset	Ground truth y_i	Noise source X
S_1	RealEEG	RealEMG
S_2	RealEEG	SimEMG
S_3	SimEEG	RealEMG
S_4	SimEEG	SimEMG

In addition, we considered that the noise measurements matrix (EMG input to the RLS filter) is not the same matrix used for contamination (CX). This is based on the assumption that the EMG electrodes are relatively far from the true muscular sources X and the measured data reflects a different mixture of those CX that yielded the artifact a. Let $\tilde{X} = JX$ be the measurement matrix, used as input of the ERLS filter in the proposed algorithm. The shape of J (and therefore $\tilde{X}$) is used to control the number of EMG channels available for the measure, mixing the sources into less (or more) channels. In this paper, three shapes of J were considered to assess the influence of the number of channels of measurement in the performance of artifact removal: $2 \times N_M$, $4 \times N_M$, and $8 \times N_M$. Fig. 4 presents a sample of the difference between both arrays for a 8×8 simulation. We also draw a new random matrix J for every window, to increase the difficulty of the estimation problem. These simulation conditions will be discussed in the results section.

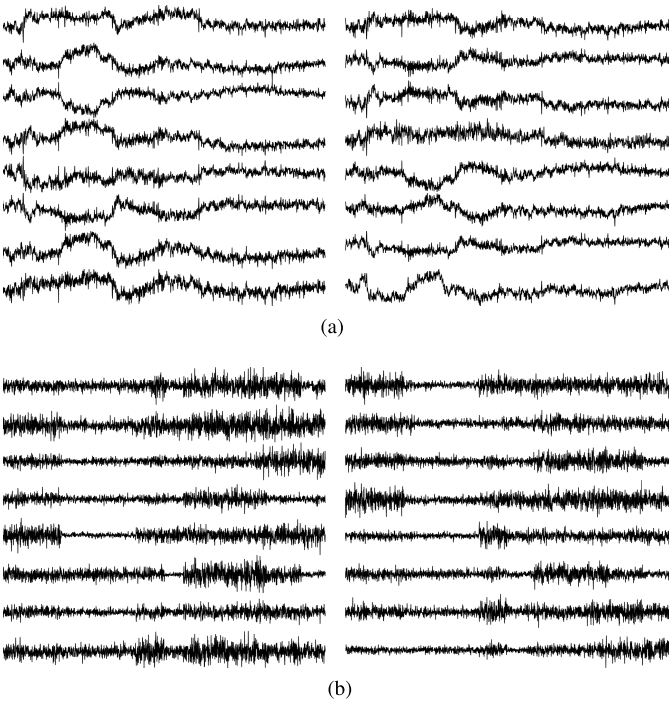

Fig. 4. Sample of 4-s window of CX (left) and JX (right), for (a) RealEMG and (b) SimEMG. CX is the matrix whose sum of rows yield the artifact a that interferes the clean signals. JX is the EMG measurements used as the reference signal in the ERLS filter.

B. Performance Comparison

The three variations of the proposed algorithm (EEMD-CCA + regression with two-, four-, and eight-EMG channels) were compared with the original algorithm (EEMD-CCA) and another recently published algorithm that reported better results than EEMD-CCA for muscular noise, namely, SuBAR [30].

A performance comparison was done in the time domain and frequency-domain using the following metrics:

1) Relative Root Mean Squared Error: The relative root mean squared error (RRMSE) of reconstructing the ground truth signals is defined as

$$\text{RRMSE} = \frac{\text{rms}(y_i - \hat{y}_i)}{\text{rms}(y_i)} \tag{14}$$

where y_i represents the ground truth and $\hat{y}_i$ represents the recovered signal for a given algorithm. The same error measure is used to compare the error on reconstructing the ground truth spectra between 0 and 50 Hz.

2) Power Difference in Information Bands: In order to quantify the expected distortion in the EEG spectral bands, we computed the difference of spectral power between the ground truth and the recovered signal in each band. The EEG information bands under consideration were: δ-band (0–4 Hz), θ-band (4–8 Hz), α-band (8–12 Hz), β-band (12–30 Hz), and γ-band (30–40 Hz). To calculate each frequency band power, we normalized the squared Fast Fourier transform (FFT) (with 2048 samples) by the average power between 40 and 50 Hz, where our signals did not show any activity of interest for this method, neither in RealEEG nor SimEEG. At the same time, this procedure allowed us to avoid the 50-Hz powerline notch filter.

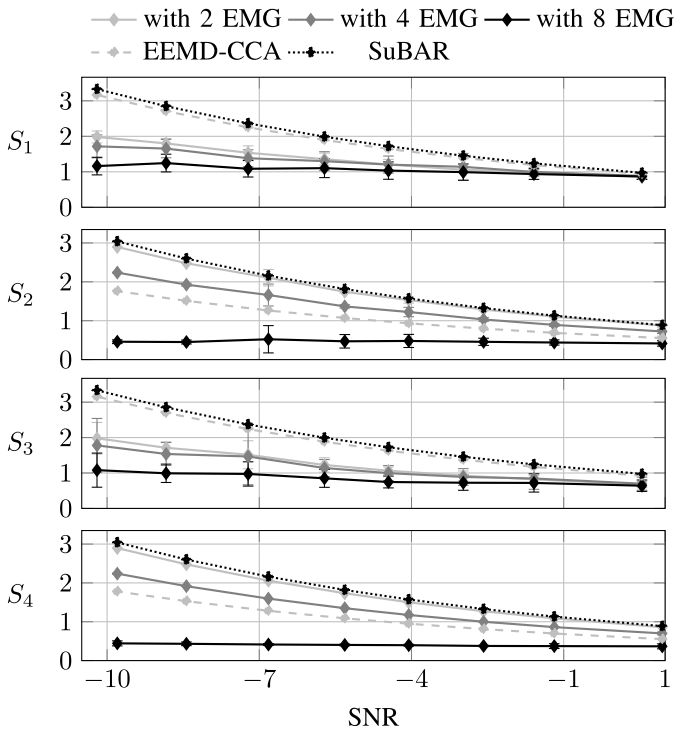

Fig. 5. RRMSE in time domain as a function of the SNR. The averages are taken across all windows and then across all electrodes. Intervals indicate the average standard deviation across electrodes.

IV. Results

We applied all the methods for comparison to each data set S_1, S_2, S_3, and S_4, consisting of 25 windows, 4 s each. A parameter grid was constructed in order to optimize the parameters of the ERLS filter, by selecting the parameters that achieved the best performance (in terms of RRMSE). The chosen parameters were $q = 10^{-4}$, $\lambda = 0.999$, and $A = I$, with initial conditions $\Theta(0) = 0$ and $P(0) = I$. Parameters of EEMD-CCA, such as the number of IMFs and the autocorrelation threshold were set to resemble the literature testing these methods, i.e., setting the IMFs number to 12 and the autocorrelation threshold to 0.9 [19], [23].

Fig. 5 presents the average RRMSE across all electrodes. Fig. 6 presents a sample window for the recovery of ground truth (in the time domain) for each data set and for every algorithm. The results for the RRMSE in the frequency domain are not shown due to that is essentially the same for the time domain, as the squared FFT is a linear transformation of the signal up to 50 Hz.

A sample of the spectral recovery for one electrode is shown in Fig. 7, where is shown that the clean, noisy, and recovered power spectral density up to 50 Hz. The power difference in all information bands is presented in Table II.

Spectral composition and characteristics of RealEEG and SimEEG are very similar, so we divided our analysis comparing real and simulated EMG signals.

A. Real EMG Signals

The distortions induced by RealEMG signals are characterized by DC fluctuations and white noise. As shown in Fig. 6 (S_1 and S_3), both EEMD-CCA and SuBAR failed to overcome the DC fluctuations while our method could successfully follow the slow variations as noise. In terms of RRMSE, all methods performed very similar for good SNRs (SNR $>$ 0 dB), and as SNR became lower, the differences between our variations of EEMD-CCA and the original algorithm increased. The original EEMD-CCA performed almost equally to SuBAR along all SNRs, having an RRMSE average between 2 and 3 for SNR < -5 dB while in all of our variations became at most 2 for the worst SNR. EEMD-CCA with eight-channel EMG filtering was the only algorithm that achieved an RRMSE average below 1 (SNR > -3 dB in real EEG signals and SNR > -6 dB in simulated EEG signals), and presented the most stable behavior (low slope). Visually in the spectral domain, in the sample shown in Fig. 7, it can be seen that our algorithm was the only one that could recover the spectra successfully. The spectral recovery is quantified (for the information bands) in Table II, where our variations showed the smaller averages and standard deviations.

TABLE II
Power Difference in Information Bands

Dataset	Band	SuBAR	EEMD-CCA	w/ 8 EMG
S_1	δ	4.2±2.5	4.7±2.7	9.7±3.1
	θ	7.5±3.1	8.2±3.4	7.9±3.1
	α	9.3±2.6	9.9±2.7	7.5±2.5
	β	4.6±2.2	5.2±2.4	3.9±2.0
	γ	1.5±0.9	1.6±0.9	1.6±0.8
S_2	δ	11.8±3.7	11.4±3.7	4.9±2.3
	θ	10.3±3.7	9.9±3.7	4.8±2.3
	α	11.3±3.0	11.0±3.0	4.9±2.2
	β	5.2±2.4	4.9±2.3	3.3±1.7
	γ	1.7±0.8	1.5±1.0	1.2±0.7
S_3	δ	10.0±5.6	9.8±5.8	5.8±5.2
	θ	7.1±5.6	7.1±5.8	4.7±4.5
	α	6.2±5.1	6.1±5.4	4.0±4.3
	β	3.8±4.3	3.9±4.5	2.4±3.5
	γ	1.5±2.0	1.6±2.1	1.3±1.8
S_4	δ	4.9±5.7	4.8±5.7	1.5±2.9
	θ	5.7±5.7	5.7±5.6	1.6±2.9
	α	5.1±5.6	5.1±5.5	1.7±2.9
	β	4.0±4.5	4.0±4.4	1.4±2.8
	γ	1.9±2.1	1.5±2.0	0.8±1.8

* Calculated as the difference between recovered and original power in dB, average±std dev. on all channels and SNRs.

B. Simulated EMG Signals

Our simulated EMG noise is characterized as a white noise with bursting behavior. In the time domain, results for S_2 and S_4 were similar to the data sets employing RealEMG signals, with the difference that results for S_2 and S_4 in the original EEMD-CCA performed better than SuBAR and our variations, with two and four EMG electrodes, for all SNRs. Again, EEMD-CCA with eight-channel EMG filtering outperformed all other methods by presenting a highly stable RRMSE average of 0.5 approximately, across all SNRs. In terms of spectral recovery (Table II), the best results were obtained for S_4 (simulated EEG and EMG), where the spectral difference in all bands never was higher than 1, followed by S_2 (simulated EEG with real EMG).

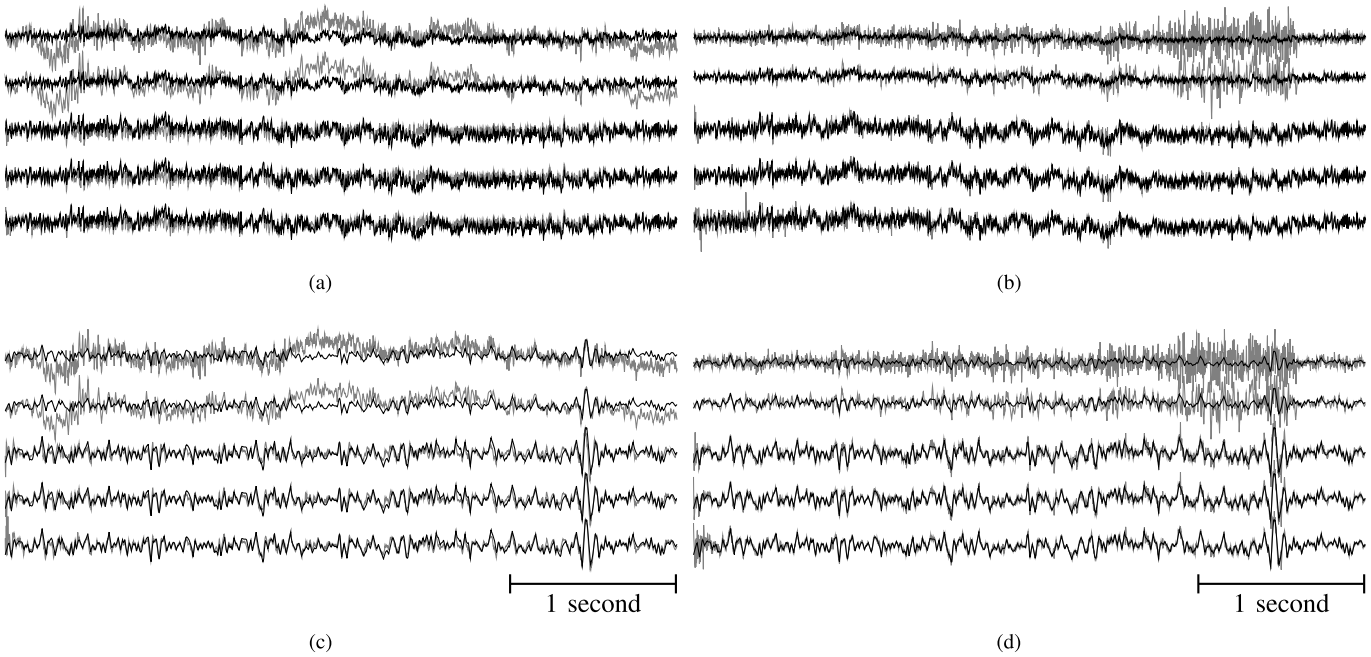

Fig. 6. Sample window of clean (black) and recovered (gray) signals for all methods and data sets, at the worst SNR, electrode O2. (a) S_1. (b) S_2. (c) S_3. (d) S_4. SuBAR, EEMD-CCA, and EEMD-CCA with two-channel EMG, four-channel EMG, and eight-channel EMG (top to bottom).

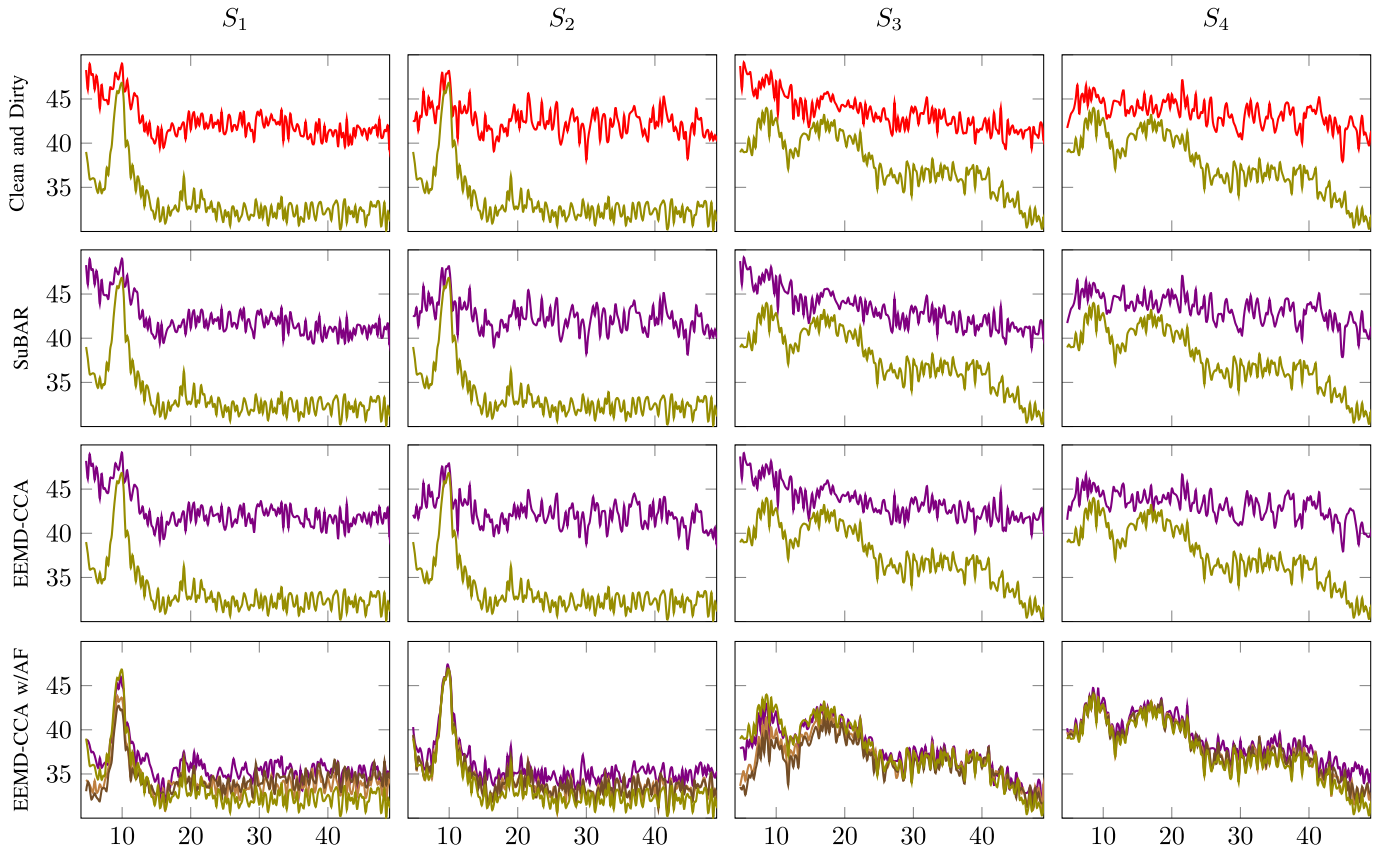

Fig. 7. Average spectra over all windows for the worst SNR of clean, noisy, and recovered signals between 0 and 50 Hz (O2 channel). The first row shows the spectra for the original (in olive) and postcontamination (in red) data set. The rest of the rows shows the recovered spectra by the algorithms (in violet) and the original spectra (in olive). In our algorithm, the 2-EMG and 4-EMG variations are in brown and dark brown colors, respectively.

Further Extension: We asked whether adding more statistically relevant information to the adaptive filter could improve the performance of the method here proposed. The assumption that a fixed number of muscular sources interfere with clean brain signals is ideal in the sense that muscles activation arises from an undetermined number of locations and sources.

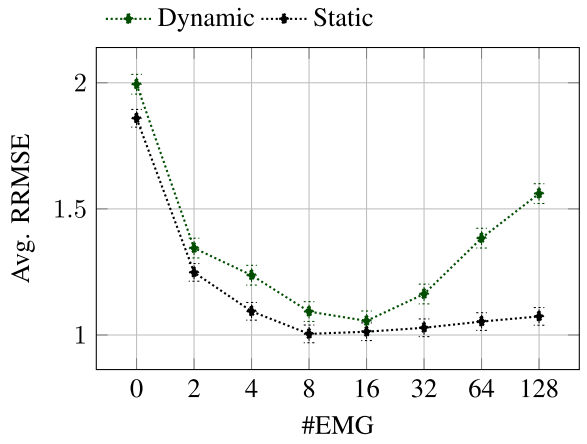

Fig. 8. Average RRMSE in the time-domain, for all electrodes, SNRs, as a function of the number of EMG electrodes used for the two simulation scenarios, dynamic (green) and static (black) mixing matrices.

The performance gain (as the number of EMG channels grow from 2 to 8) can be justified as the number of EMG electrodes for filtering (measurement matrix) is approaching the number of muscular sources that originally contaminated the ground truth.

To investigate the effect of the number of muscular sources and EMG electrodes on the behavior of our results, we further extended the simulations by enlarging C and J matrices up to $32 \times N_M$ and $128 \times N_M$, respectively, to obtain a contamination matrix CX of $N_S = 32$ sources and an EMG measurement matrix $\tilde{X}$ of #EMG $= 128$ channels. However, the number of original sources was not modified, so this tweak can be seen as taking the same original information and representing it (for contamination and filtering) in a sparser way. Furthermore, we investigated the effect of changing the matrices J and C for every window and ran simulations with static J and C matrices for the enlarged problem.

Fig. 8 shows the RRMSE averages for all EEG electrodes and N_S, as a function of the number of EMGs used for measurement (shape of J), in the two scenarios of dynamic and static mixing matrices J and C. In the case of dynamic mixing matrices, it is observed that performance degradation as the number of EMG channels increases. We attribute this effect of performance degradation to the hardness of the estimation problem in this scenario; specifically, the number of EMGs is directly related to the size of the covariance matrix and the regression coefficients inside the ERLS algorithm (noted P and Θ). P is not symmetric, and the estimation problem in this scenario changes every 2048 samples; therefore, a longer window length is required as the number of EMG channels increases. In the second case of static mixing matrices, this effect is not observed and the RRMSE remains stable, as the EMG array becomes larger.

In an experimental setting, it is worth noticing that the EEG and the EMG signals must be recorded with the same acquisition system, or applying a precise synchronization technique between them, in order to account for the instantaneous reflection effect.

V. Conclusion

In this paper, we introduce a novel method for incorporating multisensor statistical information of the noise source for BSS-based muscular artifact removal methods. We argue that adaptive regression on the resulting sources helps to mitigate both instantaneous reflections and spectral overlap. Using real and synthetic signals, we measured the performance gain for various conditions, including under massive noisy environments (SNR $<$ 0 dB). Our results show that independently of the number of muscular sources, a substantial performance improvement is expected by placing additional EMG electrodes over the face and neck muscles. The number of optimal EMG channels must be associated with the number of SMU units interfering the signal. In our case, when adding over 16 EMG electrodes, the filter becomes unable to capture muscular source characteristics. Furthermore, increasing the number of channels required additional samples in a window to achieve good estimations of the covariance matrix, thus indicating a tradeoff between the number of EMGs used and the hardness of the estimation problem. Although EEMD-CCA and SuBAR performed almost equally in all scenarios, there is an advantage of EEMD-CCA over SuBAR, as EEMD-CCA can be intuitively extended to account for the hallmarks of the muscle interference problem we mentioned, namely, spectral overlap (partially separated by BSS) and zero-lag interference (mitigated by the ERLS algorithm). On the other hand, SuBAR is an algorithm that relies its effectivity on replacing wavelets coefficients of random realizations of a signal, thus, extending this algorithm to account hallmarks of the specific problem could be confusing. For this reason, we argue that SuBAR is designed as a general-purpose artifact removal algorithm, whereas EEMD-CCA with AF is specific for the muscle problem interference.

Therefore, we recommend the placement of EMG electrodes over muscles expected to produce activity in an experimental scenario, and thus, to automate BSS-based algorithms, as it is a computationally inexpensive enhancement that could substantially reduce the distortions induced by voluntary and involuntary muscular activations.

References

[1] M. M. Mannan, M. A. Kamran, and M. Y. Jeong, "Identification and removal of physiological artifacts from electroencephalogram signals: A review," *IEEE Access*, vol. 6, pp. 30630–30652, 2018.

[2] K. Paluch *et al.*, "Beware: Recruitment of muscle activity by the EEG-neurofeedback trainings of high frequencies," *Frontiers Hum. Neurosci.*, vol. 11, p. 119, Mar. 2017. doi: 10.3389/fnhum.2017.00119.

[3] G. Yilmaz, P. Ungan, O. Sebik, P. Uginčius, and K. S. Turker, "Interference of tonic muscle activity on the EEG: A single motor unit study," *Frontiers Hum. Neurosci.*, vol. 8, p. 504, Jul. 2014. doi: 10.3389/fnhum.2014.00504.

[4] E. M. Whitham *et al.*, "Scalp electrical recording during paralysis: Quantitative evidence that EEG frequencies above 20 Hz are contaminated by EMG," *Clin. Neurophysiol.*, vol. 118, no. 8, pp. 1877–1888, Aug. 2007. doi: 10.1016/j.clinph.2007.04.027.

[5] J. A. Boytsova, S. G. Danko, and S. V. Medvedev, "When EMG contamination does not necessarily hide high-frequency EEG: Scalp electrical recordings before and after dysport injections," *Experim. Brain Res.*, vol. 234, no. 11, pp. 3091–3106, Nov. 2016. doi: 10.1007/s00221-016-4708-3.

[6] I. I. Goncharova, D. J. McFarland, T. M. Vaughan, and J. R. Wolpaw, "EMG contamination of EEG: Spectral and topographical characteristics," *Clin. Neurophysiol.*, vol. 114, no. 9, pp. 1580–1593, Sep. 2003. doi: 10.1016/s1388-2457(03)00093-2.

[7] W. D. Clercq, A. Vergult, B. Vanrumste, W. Van Paesschen, and S. V. Huffel, "Canonical correlation analysis applied to remove muscle artifacts from the electroencephalogram," *IEEE Trans. Biomed. Eng.*, vol. 53, no. 12, pp. 2583–2587, Nov. 2006. doi: 10.1109/tbme.591-2006.879459.
[8] A. J. Shackman, B. W. McMenamin, H. A. Slagter, J. S. Maxwell, L. L. Greischar, and R. J. Davidson, "Electromyogenic artifacts and electroencephalographic inferences," *Brain Topogr.*, vol. 22, no. 1, pp. 7–12, Feb. 2009. doi: 10.1007/s10548-009-0079-4.
[9] B. W. McMenamin, A. J. Shackman, J. S. Maxwell, L. L. Greischar, and R. J. Davidson, "Validation of regression-based myogenic correction techniques for scalp and source-localized EEG," *Psychophysiology*, vol. 46, no. 3, pp. 578–592, May 2009. doi: 10.1111/j.1469-8986.2009.00787.x.
[10] B. W. McMenamin *et al.*, "Validation of ICA-based myogenic artifact correction for scalp and source-localized EEG," *NeuroImage*, vol. 49, no. 3, pp. 2416–2432, Feb. 2010. doi: 10.1016/j.neuroimage.2009.10.010.
[11] S. Olbrich, J. Jödicke, C. Sander, H. Himmerich, and U. Hegerl, "ICA-based muscle artefact correction of EEG data: What is muscle and what is brain?: Comment on McMenamin et al.," *NeuroImage*, vol. 54, no. 1, pp. 1–3, Jan. 2011. doi: 10.1016/j.neuroimage.2010.04.256.
[12] B. W. McMenamin, A. J. Shackman, L. L. Greischar, and R. J. Davidson, "Electromyogenic artifacts and electroencephalographic inferences revisited," *NeuroImage*, vol. 54, no. 1, pp. 4–9, Jan. 2011. doi: 10.1016/j.neuroimage.2010.07.057.
[13] K. T. Sweeney, H. Ayaz, T. E. Ward, M. Izzetoglu, S. F. McLoone, and B. Onaral, "A methodology for validating artifact removal techniques for physiological signals," *IEEE Trans. Inf. Technol. Biomed.*, vol. 16, no. 5, pp. 918–926, Sep. 2012. doi: 10.1109/titb.2012.2207400.
[14] B. Mijovic, M. De Vos, I. Gligorijevic, J. Taelman, and S. Van Huffel, "Source separation from single-channel recordings by combining empirical-mode decomposition and independent component analysis," *IEEE Trans. Biomed. Eng.*, vol. 57, no. 9, pp. 2188–2196, Sep. 2010. doi: 0.1109/tbme.2010.2051440.
[15] K. T. Sweeney, S. F. McLoone, and T. E. Ward, "The use of ensemble empirical mode decomposition with canonical correlation analysis as a novel artifact removal technique," *IEEE Trans. Biomed. Eng.*, vol. 60, no. 1, pp. 97–105, Jan. 2013. doi: 10.1109/tbme.2012.2225427.
[16] M. M. N. Mannan, M. Y. Jeong, and M. A. Kamran, "Hybrid ICA—Regression: Automatic identification and removal of ocular artifacts from electroencephalographic signals," *Frontiers Hum. Neurosci.*, vol. 10, p. 193, May 2016.
[17] A. Hyvärinen and E. Oja, "Independent component analysis: Algorithms and applications," *Neural Netw.*, vol. 13, no. 4, pp. 411–430, 2000.
[18] X. Chen, H. Peng, F. Yu, and K. Wang, "Independent vector analysis applied to remove muscle artifacts in EEG data," *IEEE Trans. Instrum. Meas.*, vol. 66, no. 7, pp. 1770–1779, Jul. 2017.
[19] X. Chen, A. Liu, J. Chiang, Z. J. Wang, M. J. McKeown, and R. K. Ward, "Removing muscle artifacts from EEG data: Multichannel or single-channel techniques?" *IEEE Sensors J.*, vol. 16, no. 7, pp. 1986–1997, Apr. 2016. doi: 10.1109/JSEN.2015.2506982.
[20] A. K. Maddirala and R. A. Shaik, "Separation of sources from single-channel eeg signals using independent component analysis," *IEEE Trans. Instrum. Meas.*, vol. 67, no. 2, pp. 382–393, Feb. 2018.
[21] B. Azzerboni, F. La Foresta, N. Mammone, and F. Morabito, "A new approach based on wavelet-ICA algorithms for fetal electrocardiogram extraction," in *Proc. ESANN 13th Eur. Symp. Artif. Neural Netw.*, 2007, pp. 193–198.
[22] A. K. Maddirala and R. A. Shaik, "Removal of EOG artifacts from single channel EEG signals using combined singular spectrum analysis and adaptive noise canceler," *IEEE Sensors J.*, vol. 16, no. 1, pp. 8279–8287, Dec. 2016. doi: 10.1109/jsen.2016.2560219.
[23] X. Chen, X. Xu, A. Liu, M. J. Mckeown, and Z. J. Wang, "The use of multivariate EMD and CCA for denoising muscle artifacts from few-channel EEG recordings," *IEEE Trans. Instrum. Meas.*, vol. 67, no. 2, pp. 359–370, Feb. 2018.
[24] Z. Wu and N. E. Huang, "Ensemble empirical mode decomposition: A noise-assisted data analysis method," *Adv. Adapt. Data Anal.*, vol. 1, no. 1, pp. 1–41, 2008. doi: 10.1142/s1793536909000047.
[25] P. J. J. Luukko, J. Helske, and E. Räsänen, "Introducing libeemd: A program package for performing the ensemble empirical mode decomposition," *Comput. Statist.*, vol. 31, no. 2, pp. 545–557, Jul. 2015. doi: 10.1007/s00180-015-0603-9.
[26] R. Oostenveld, P. Fries, E. Maris, and J.-M. Schoffelen, "FieldTrip: Open source software for advanced analysis of MEG, EEG, and invasive electrophysiological data," *Comput. Intell. Neurosci.*, vol. 2011, Jan. 2011, Art. no. 1. doi: 10.1155/2011/156869.
[27] M. A. Klados, C. Papadelis, C. Braun, and P. D. Bamidis, "REG-ICA: A hybrid methodology combining blind source separation and regression techniques for the rejection of ocular artifacts," *Biomed. Signal Process. Control*, vol. 6, no. 3, pp. 291–300, Jul. 2011. doi: 10.1016/j.bspc.2011.02.001.
[28] W. Liu, I. Park, Y. Wang, and J. C. Príncipe, "Extended kernel recursive least squares algorithm," *IEEE Trans. Signal Process.*, vol. 57, no. 10, pp. 3801–3814, Oct. 2009. doi: 10.1109/tsp.2009.2022007.
[29] D. A. Bridwell, S. Rachakonda, R. F. Silva, G. D. Pearlson, and V. D. Calhoun, "Spatiospectral decomposition of multi-subject EEG: Evaluating blind source separation algorithms on real and realistic simulated data," *Brain Topography*, vol. 31, no. 1, pp. 47–61, Jan. 2018. doi: 10.1007/s10548-016-0479-1.
[30] M. Chavez, F. Grosselin, A. Bussalb, F. D. V. Fallani, and X. Navarro-Sune, "Surrogate-based artifact removal from single-channel EEG," *IEEE Trans. Neural Syst. Rehabil. Eng.*, vol. 26, no. 3, pp. 540–550, Mar. 2018. doi: 10.1109/tnsre.2018.2794184.

Juan Andrés Mucarquer received the P.E. degree in telematics engineering and the M.S. degree in electronic engineering from Universidad Técnica Federico Santa María, Valparaíso, Chile. He is currently pursuing the Ph.D. degree in linguistics with Macquarie University, Sydney, NSW, Australia.

He worked at the Advanced Center for Electrical and Electronic Engineering (AC3E), Universidad Técnica Federico Santa María and he is currently with the Australian Hearing Hub, Macquarie University, where his current research is centered on the mechanisms of statistical learning in auditory perception. His research interests include computational neuroscience and biological cybernetics.

Pavel Prado received the M.Sc. degree in Comparative Physiology from the Faculty of Biology, University of Havana, Havana, Cuba, and the Ph.D. degree in Health Sciences from the University of Medical Sciences, Havana.

He is currently a Post-Doctoral Fellow with the Advanced Center for Electrical and Electronic Engineering (AC3E), Universidad Técnica Federico Santa María, Valparaiso, Chile. His current research interests include the auditory feedback on the control of vocal production, using electrophysiological techniques (electroencephalography and electromyography). His research is currently supported by CONICYT in Chile.

María-José Escobar received the Ph.D. degree in signal and image processing from INRIA Sophia-Antipolis, Université Nice Sophia-Antipolis, Nice, France, and the M.S. and P.E. degrees in electronic engineering from Universidad Técnica Federico Santa María, Valparaíso, Chile.

She is currently an Associate Professor with the Department of Electronic Engineering, Universidad Técnica Federico Santa María, and an a principal Researcher with the Advanced Center of Electrical and Electronic Engineering (AC3E), Valparaíso. Her current research interests include biological vision, computational neuroscience, and cognitive robotics. She is currently studying computational strategies performed by the mammalian retina, specially related to motion processing. Her research is currently supported by AFOSR in the U.S. and CONICYT in Chile.

Wael El-Deredy received the B.Sc. and M.Sc. degrees in electrical and electronics engineering from Ain Shams University, Cairo, Egypt, and Imperial College London, London, U.K., respectively, and the Ph.D. degree in neurocomputing from University College London, London.

He is currently a Professor of computational neuroscience at Universidad de Valparaiso and Associate Researcher with the Advanced Center for Electrical and Electronic Engineering, Universidad Técnica Federico Santa María, Valparaíso, Chile. His research interests include probabilistic models of brain function, the development of novel methods for neuroimaging and application for neuroengineering and neuroprostatics. His research is supported by the MRC and EPSRC in the U.K. and CONICYT in Chile.

Matías Zañartu (S'08–M'11–SM'18) received the B.S. degree in acoustical engineering from Universidad Tecnológica Vicente Pérez Rosales, Santiago, Chile, and the M.S. and Ph.D. degrees in electrical and computer engineering from Purdue University, West Lafayette, IN, USA.

He is currently an Associate Professor with the Department of Electronic Engineering and also the Director of the Advanced Center for Electrical and Electronic Engineering, Universidad Técnica Federico Santa María, Valparaíso, Chile. His current research interests include the development of digital signal processing, system modeling, and biomedical engineering tools that involve speech, hearing, and acoustics. His recent research efforts have revolved around developing quantitative models that describe nonlinear effects in human speech production, and applying these physiological descriptions for the development of communication and clinical technologies. His research is currently supported by NIH in the U.S. and CONICYT in Chile. Dr. Zañartu is a Fulbright Fellow.